CINEMATOGRAPHIC ANALYSIS OF A SINGLE BUBBLE COLLAPSE FLOW INDUCED BY PRESSURE WAVE

Shenq-Yuh Jaw [1], Whey-Fone Tsai[2], and Robert R. Hwang[3]

ABSTRACT

In this study, a single cavitation bubble is generated by rotating a U-tube filled with water. A series of bubble collapse flows induced by pressure waves of different strengths are investigated by positioning the cavitation bubble at different stand-off distances to the solid boundary. It is found that the Kelvin-Helmholtz vortices are formed when the liquid jet induced by the pressure wave penetrates the bubble surface. If the bubble center to the solid boundary is within one to three times the bubble's radius, a stagnation ring will form on the boundary when impacted by the penetrated jet. The liquid inside the stagnation ring is squeezed toward the center of the ring to form a counter jet after the bubble collapses. At the critical position, where the bubble center from the solid boundary is about three times the bubble's radius, the bubble collapse flows will vary. Depending on the strengths of the pressure waves applied, either just the Kelvin-Helmholtz vortices form around the penetrated jet or the penetrated jet impacts the boundary directly to generate the stagnation ring and the counter jet flow. If the bubble surface is in contact with the solid boundary, the liquid jet can only splash radially without producing the stagnation ring and the counter jet. The complex phenomenon of cavitation bubble collapse flows are clearly manifested in this study.

Keywords: Cavitation, bubble collapse, counter jet

INTRODUCTION

It is well known that the collapse of the cavitation bubbles in the fluid flow can cause serious damage on pipes, hydraulic structures and turbo-machineries. The generation and the collapse of the cavitation bubble are induced by the variation of its surrounding velocity and pressure fields. If the collapse of cavitation bubbles occurs near the solid boundary, the water hammer impact to the boundary can be induced (Plesset and Chapman 1971). The shock wave produced by the bubble collapse can possibly damage the solid boundary causing the destruction of structures.

How these tiny cavitation bubbles can cause the serious structural damage has surely caught the attention and curiosity of researchers. Many of them have plunged into the study of the characteristics of

---

[1] Corresponding author: Department of Systems Engineering And Naval Architecture, National Taiwan Ocean University, e-mail: syjaw@ntou.edu.tw

[2] National Center of High Performance Computing

[3] Institute of Physics, Academia Sinica

the bubble collapse flow and its effect on the destruction of its surrounding solid boundary. These studies include the generation of shock wave, cavitation luminescence, and liquid jet flow, etc. If the cavitation bubble is located near a solid boundary, a counter-jet flow will also be induced. However, there has not been a firm conclusion yet for how these tiny cavitation bubbles can cause the destruction on the solid boundary.

Rayleigh (1917) studied the erosion of high speed propeller blade subjected to the effect of cavitation bubble. He developed the dynamic theory for the collapse of spherical bubbles and derived the Rayleigh equation. Many following researchers carried out related researches based on this theory. Plesset (1949) considered the influence of fluid viscosity and surface tension and derived the Rayleigh-Plesset equation. Gilmore (1952) further considered the influence of the compressibility of fluid on the bubble collapse flow. The influence of the thermal conductivity of the fluid was considered in the study of Plesset and Zwick (1952). Their research results showed that the bubble collapse flow can be assumed to be an adiabatic process since the bubble collapse time is very short and the influence of the thermal conduction can be neglected.

Kornfeld and Suvorov (1944) mentioned that when the bubble collapsed near a solid boundary, the bubble is deformed to a non-spherical shape and a liquid jet flow is generated. This phenomenon was proved in the experiment carried out by Naude & Ellis (1961). The numerical model of Plesset and Chapman (1971) also revealed this phenomenon. Benjamin and Ellis (1966) and Philipp and Lauterborn (1998) also studied the bubble collapse flow and the consequent damage on the solid boundary. The impact of the liquid jet on the solid boundary was once thought to be the cause of the boundary damage. However, recent research results reveled that there are more important factors other than the impact of the liquid jet that causes the boundary damage.

The pressure variation induced by the bubble collapse flow was first investigated by Rayleigh (1917). The noise generated by the bubble collapse near solid boundary was discovered by Harrison (1952). Vogel and Lauterborn (1988) found a close relationship between the pressure pulse and the stand-off distance between the bubble and the rigid boundary. The bubble collapse results in a very high pressure. The pressure pulse then revolves into a series of shock waves. The shock waves also appeared in the study of Tomita and Shima(1986); Ward and Emmony (1991); Ohl et al. (1995); Shaw et al.(1996); Lindau and Lauterborn (2003), etc.

Light can be emitted, especially when the bubble collapse occurs in the flow with lower fluid viscosity or higher pressure flow field. Under these conditions, the bubble collapse time is relatively short; it is easier for the gas inside the bubble to be heated to the light emitted temperature (McCarn et al 2006). Ohl et al. (1998) also found the emission of light for the bubble collapse near the solid boundary. This phenomenon is called the "Single Cavitation Bubble Luminescence (SCBL)". Buzukov & Teslenko (1971) and Akmanov et al. (1974) also reported similar results. The strength of the SCBL is closely related to the stand-off distance to the solid boundary (Ohl et al 1999). The researches related to the SCBL in recent years include the studies of Wolfrum et al. (2001), Baghdassarian et al. (2001). Akhatov et al. (2001) proposed the bubble dynamics mathematical model for a laser induced, spherically symmetric cavitation bubble.

Counter jet is generated when the bubble collapsed near the solid boundary. The formation and growth of the counter jet is very rapid. Nevertheless, the counter jet can exist for a while after it is formed. The counter jet was found in the experiments of Harrison (1952), and Kling and Hammitt (1972); however it was until Lauterborn (1974) who first described the counter jet phenomenon. The origin of the counter jet is not known yet with certainty. Counter jet did not appear in the numerical simulations of Best (1993), Zhang et al. (1993), Blake et al. (1997), while it did appear in the experiments of Philipp and Lauterborn

(1998), Tomita and Shima (1986), Vogel et al. (1989), Ward and Emmony (1991), Kodama and Tomita (2000). The discrepancy between the numerical simulations and the experimental results leads to the assumption that the counter jet may not be part of the bubble collapse flow, but generated by a complicated mechanism during the bubble collapse. If the bubble is in contact with the solid boundary, the counter jet will not be generated. Since the shock wave and the counter jet are generated at the final stage of the bubble collapse, the formation of counter jet is thus considered to be coupled to the shock wave scenario during bubble collapse.

According to the study of Vogel et al. (1989), whether the counter jet will occur or not during the bubble collapse is dependent on the stand-off distance from the center of the bubble to the solid boundary: $\gamma = \dfrac{d}{R_{max}}$, where R_{max} is the maximum radius of the bubble and d is the distance between the bubble center and the solid boundary. When γ falls in the range of $1 < \gamma \leq 3$, counter jet is observed. However, no counter jet is generated under the condition of $\gamma > 3$. Lindau and Lauterborn (2003) investigated the relationships between the counter jet rebound height, the bubble collapse time and their respective γ values. Their results revealed an increasing γ for a smaller rebound height, and a shorter time of collapse.

According to the Rayleigh's equation, the relationship between the bubble collapse time and the bubble radius, without the boundary effect, is: $R_{max} = 1.09 \sqrt{\dfrac{p - p_v}{\rho}} \, t_c$, where p and ρ are the pressure of the flow field and the fluid density at ambient temperature respectively, p_v is the vapor pressure, t_c is the bubble collapse time. If solid boundary exists, the bubble collapse time is longer. Generally the size of the cavitation bubble generated in the laboratory is about 1.5 mm in radius. For a laser induced spherical bubble, the bubble collapse time is around $150\,\mu s$. Since the bubble size is small, the bubble collapse time is short, the bubble collapse flow is complicate, and the generation of a single cavitation bubble at a specific position is not easy, very expensive equipments is generally required to perform the bubble collapse flow measurements. The high speed cameras with framing rates ranging between several thousand to 100 million frames per second were adopted in many researches. The particle image velocimetry (PIV) was also adopted to measure the velocity field of the bubble collapse flow (Vogel and Lauterborn 1998). However since the volume of the bubble was small and the bubble collapse time was short, only a rough sketch of the flow field around the cavitation bubble was obtained.

In laboratory, a single cavitation bubble is generally generated in a cuvette by the optical breakdown of the liquid using a high energy laser beam (Lauterborn 1974, 1972). The same method was used to generate a single cavitation bubble by several subsequent researches. Usually the bubble generated using this method has small volume with 1.5 mm in radius, since the bubble size is restricted by the strength of the laser energy. Note also that the bubble generated by the optical breakdown is different from the true cavitation bubble in certain aspects, such as vaporizing impurities in the solution may occur, the pressure inside the bubble is different from the cavitation vapor pressure at ambient temperature, and there is no re-condensable vapor inside the bubble, etc. Spark discharge is also adopted to generate a single bubble. However, this method has the defect that the spark generator may disturb the bubble collapse flow. Bubbles can also be injected directly into the fluid by means of a needle. Bubble collapse is induced by the high pressure, 94 MPa, shock wave generated from a lithotripter (Philipp 1993). Sankin et al.(2005) also used a lithotripter to generate a 39 MPa shock wave and successfully measured the interaction of the shock wave and the bubble collapse flow.

From the paper reviews presented above, it is perceived that the cavitation bubble collapse flow is very difficult to measure due to the facts that the bubble size is small, the collapse time is very short, and the flow induced is very complicate. In addition, as mentioned before, the bubble generated by the optical breakdown is different from a true cavitation bubble. A cavitation bubble containing re-condensable vapor, when collapsed, will produce greater energy than the ones without re-condensable vapor (Akhatov et al. 2001; Zhu and Zhong 1999). To resolve these problems, a simpler method for the generation of a true cavitation bubble is proposed in this study. By rotating a U tube filled with water, a single cavitation bubble is generated and stayed at the center of the rotational axis due to the effect of centrifugal force. The cinematographic analysis of bubble collapse flows induced by pressure waves of different strengths can thus be performed easily. By lowering the strength of the pressure wave, the bubble collapsed in a longer period of time, the characteristics of the true cavitation bubble collapse flow are clearly manifested. The present study focuses on the investigation of the formation of the liquid jet and the counter jet, at different stand-off distances to the boundary, and their consequent influences on the bubble collapse flow.

EXPERIMENTAL SETUP

The experimental set up for the generation of a single cavitation bubble and the bubble collapse flow measurements is shown in Figure 1. The DC brushless motor adopted has two horsepower maximum power output. The highest angular velocity generated is 2000 RPM. The output angular velocity can be adjusted by a digital controller.

The U-shape platform is made of 20 mm thick acrylic. Centered at the axis of the motor, the radius of the rotational arm is 250 mm long. Two vertical forearms 150 mm in height are fixed to the edge of the platform. A transparent circular tube of 200 mm in length, 5mm in internal diameter is sited on the horizontal platform. A soft PVC tube with an internal diameter of 5mm is fastened to the vertical forearm so that the measurement devices can be conveniently changed. The piston driven pressure wave generator is connected to the one end of the PVC tube. The other end of the PVC tube is connected to the transparent circular tube. On the other end of the transparent circular tube a solid boundary is connected. A hole 1 mm in diameter is drilled on the solid boundary and connected to a pressure sensor so that the strength of the pressure wave for inducing the bubble collapse flow can be measured.

The transparent circular tube on the U-shape platform is filled with water, as shown in Figure 2. On the air-water interface is the free surface boundary, where the surface pressure is one atmosphere. Therefore, at the center location of the U tube, the hydrostatic pressure is $p_0 = p_{atm} + \rho g \Delta h$, where p_{atm} is the atmospheric pressure, g is the gravitational acceleration, and Δh is the height of the water column.

When the U-tube is rotated, the fluid inside the tube is subjected to the centrifugal acceleration. The pressure distribution along the radius is a parabolic profile, as the dash-line shown in Figure 2. At the vertical forearm, although the column height Δh is slightly increased, the free surface is still kept at one atmospheric pressure. Therefore, the pressure difference between the free surface and the axis of rotation is $\rho g \Delta h - \frac{1}{2} \rho r^2 \omega^2$, where r is the radius of the rotational arm and ω is the angular velocity.
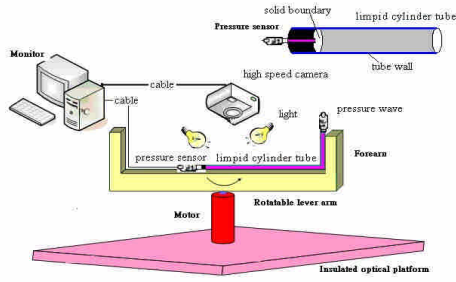
Fig. 1. experiment setup   **Fig. 2. The pressure distribution**
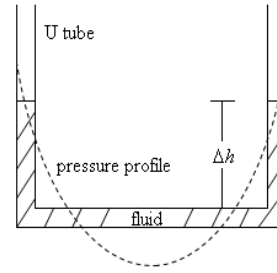
When ω is gradually increased, the pressure at the axis of rotation of the transparent circular tube is gradually decreased to the vapor pressure of ambient water temperature, a single cavitation bubble is thus generated at the central axis of the U-tube. By controlling the angular velocity of the rotating U-tube, a desirable size of a single cavitation bubble can be generated.

A Fastec high speed camera is used to record the images of bubble collapse flows. The higher the image recording speed, the lower the image resolution will be. For the image recording speed set at 4,000 frames per second, the image resolution recorded is 1280×128 pixels. A Kulite XTL-190 pressure sensor incorporated with the NATIONAL INSTRUNENTS-6221 Analog I/O card is used for the measurement of the pressure variation.

After the cavitation bubble is generated, the rotating U-tube is stopped instantly to restore the pressure back to the hydrostatic pressure. This pressure recovery alone is not enough to cause the cavitation bubble collapse. Therefore, a piston driven by a spring is used to trigger the pressure wave required for inducing the cavitation bubble collapse, by hitting the free surface of the PVC tube with the piston. Two signals are sent simultaneously to trigger the high speed camera and the computer for image and pressure data recording.

A single cavitation bubble and the subsequent bubble collapse flows induced by pressure waves are easily generated by the experimental setup proposed in this study. Cinematographic analysis of the cavitation bubble collapse flows at different stand-off distances are performed and discussed in the following.

CINEMATOGRAPHIC ANALYSIS OF THE CAVITATION BUBBLE COLLAPSE FLOWS

To investigate the characteristics of the liquid jet and the counter jet formed in the bubble collapse flow, a series of experiments at the stand-off distance $\gamma = 7, 3, 2, 1$ is performed respectively. The cavitation bubble generated is 2 mm in radius. Pressure waves of different strengths are applied to induce the bubble collapse flow. The experimental results are discussed below:

A. Bubble Collapse Flows at $\gamma \approx 7$

At this stand-off distance, the center of the cavitation bubble to the solid boundary is seven times of the bubble radius. A 160 kPa pressure wave comes from the left hand side to induce the bubble collapse flow. The formation of the liquid jet at the central axis of the cavitation bubble is shown in Figure 3. Series images from the bubble deformation to the bubble collapse are shown in Figure 3. These images clearly manifested that, for this stand-off distance, the cavitation bubble collapse flow is not affected by

the solid boundary.

As shown in Figure 3, when the bubble is concaved by the pressure wave, a liquid jet is formed at the central axis of the bubble. Initially the liquid jet is converged as the bubble surface concaved toward the center of the bubble. The left hand side bubble surface progressively moves toward the right hand side surface of the bubble. The counter force opposing the liquid jet is then gradually increased as the two bubble surfaces approach each other. At the same time, the liquid jet is accumulating energy and forming a structure that has a larger front and a smaller rear, as shown in second row of Figure 3. When sufficient energy is accumulated by the liquid jet during this continuous motion, the overlaid bubble surface is threaded and subsequently spouted into a jet flow. The Kelvin-Helmholtz instability occurs at the spouted jet surface and vortices are formed due to the presence of sufficient velocity shear between the jet flow and the surrounding static fluid, as shown in images listed in the second and the third row of Figure 4. Jaw et al. (2007) clearly demonstrated the Kelvin-Helmholtz vortex formation in their measurements of soap bubble collapse flow. The bubble threaded by the jet flow is then collapsed into two smaller bubbles. If the strength of the pressure wave is increased, the bubble is collapsed into a number of smaller bubbles. From these series of images, the features of the cavitation bubble collapse without solid boundary effect are clearly manifested.
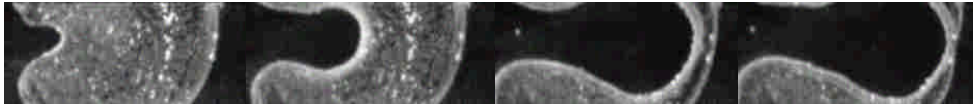
Fig. 3. Liquid jet accumulating energy in the concaved bubble

Fig. 4. Images of the bubble collapse at $\gamma \approx 7$. 1st row: bubble deformation induced by pressure wave; 2nd and 3rd row: formation of the Kelvin-Helmholtz vortices. The strength of the pressure wave is 160 kPa . The time interval between images is 1/2000 second.

B. Bubble Collapse Flows at $\gamma \approx 2$

As described in the introduction, the counter jet is generated when the stand-off distance from the center of the bubble to the solid boundary is within one to three times the bubble's radius ($1 < \gamma \leq 3$). The experiments conducted with $\gamma \approx 2$ falls within this range.

The distance from the right hand side of the bubble surface to the solid boundary is only one radius long. The Kelvin-Helmholtz vortices are generated after the bubble surface is threaded and the jet flow is formed. Images of bubble collapse flow induced by a 250 kPa pressure wave are shown in Figure 5. The height of the jet induced is long enough for the jet to impact the solid boundary, as shown in the first row of Figure 5. At the root of the jet where the bubble surface is penetrated, the velocity is high and pressure is low, the bubble is stretched towards the solid boundary, as the images shown in the second row. The counter jet is clearly presented in the first image of the third row. On the same image, it is also found that the fluid outside the bubble surface flows along the outwards radial direction. For such a flow configuration to exist there must be a stagnation ring formed when the jet impact the solid boundary, which separates the inwards and outwards radial flows. Note also that a liquid layer must exist between

the bubble surface and the solid boundary; the liquid layer can then be squeezed by the inwards radial flow to form the counter jet. For a liquid layer to exist between the bubble surface and the solid boundary, the distance from the bubble center to the boundary must be larger than the bubble radius, or the stand-off distance must be larger than one. Therefore, $\gamma > 1$ is a necessary condition for the bubble collapse flow to generate the counter jet.

If the strength of the pressure wave is increased to be 475 kPa, the bubble collapse flow and the counter jet formed is shown in Figure 6. The counter jet formed is higher and the cavitation bubble is broken into a number of small bubbles.
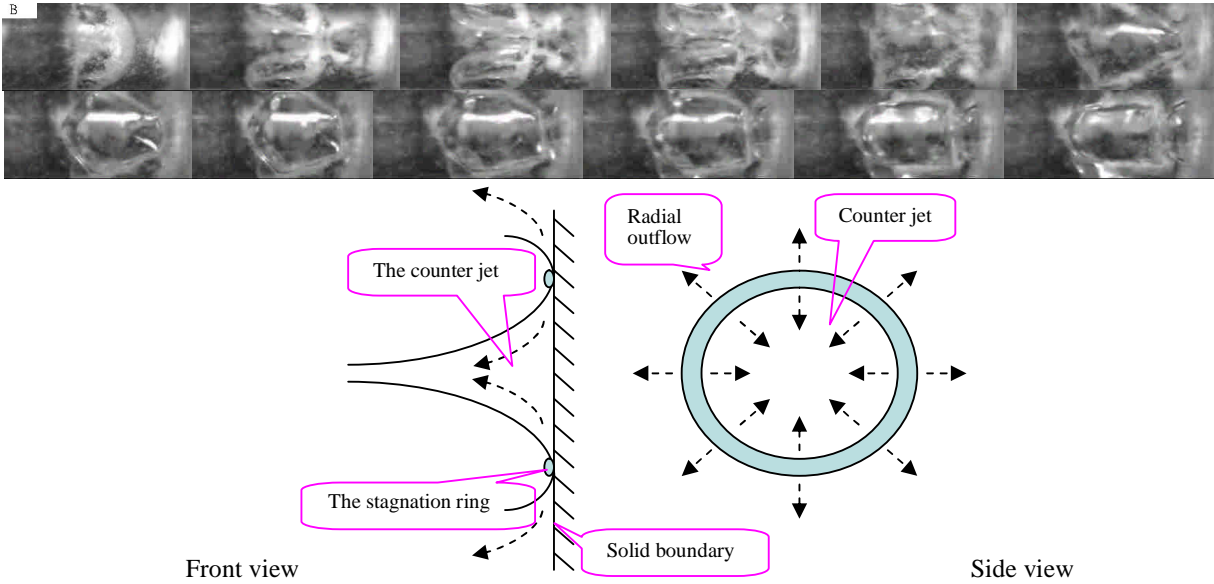
Fig. 5. Upper Part: Images of bubble collapse flow at $\gamma \approx 2$ (The counter jet is indicated by an arrow). The strength of the pressure wave is 250kPa. The time interval between images is 1/2000 second. Lower Part: Schematic diagram for the counter jet formation.

Fig. 6. Images of bubble collapse flow at $\gamma \approx 2$. The strength of the pressure wave is 475 kPa. The time interval between images is 1/2000 second.

C. Bubble Collapse Flows at $\gamma \approx 3$

The stand-off distance $\gamma \approx 3$ is a critical value for the generation of a counter jet. In this study, three different strengths of pressure waves are used to induce the cavitation bubble collapse. The influences of the pressure waves to the formation of the counter jet at this critical stand-off distance are investigated.

The images of the bubble collapse flow induced by a pressure wave of 195 kPa are shown in the first and second row of Figure 7. An inwards dent is formed and a liquid jet is generated. The bubble surface is then threaded by the liquid jet and the Kelvin-Helmholtz vortices are formed around the penetrated jet. The height of the penetrated jet is not long enough to impact the solid boundary. Similar to the results presented for the stand-off $\gamma \approx 7$, the counter jet is not generated in this bubble collapse flow.

If the strength of the pressure wave is increased to 265kPa, it is found from the images in the third row of Figure 7 that the penetrated jet can barely touch the solid boundary. Unlike the semi-hemispheric front of the penetrated jet induced by lower pressure wave, as shown in the first and second rows of Figure 7, the front of the penetrated jet is flat, a clear evidence that the solid boundary effect has come into play. In the meantime, the jet started to spread radially so that the circumference of the spread jet touch the tube wall before the jet front impacts the solid boundary. This spreading jet keeps moving towards the right side until it touches the solid boundary. The impact jet is then rebounded, as the images shown in the fourth row of Figure 7. Although the penetrated jet induced by this strength of pressure wave can impact the solid boundary, the jet has already spread and touched the surrounding tube wall, disabling the penetrated jet from forming the stagnation ring and the counter jet. Note that the bubble is also stretched and deformed towards its right side due to the pressure variation of the bubble collapse process, as the images shown in the fifth and sixth rows of Figure 7. If the strength of the pressure wave is increased to 550 kPa, the penetrated jet is able to impact the solid boundary directly to form the stagnation ring and the counter jet, as shown in the last two rows of Figure 7.

Fig. 7. Images of bubble collapse at $\gamma \approx 3$. The 1st and 2nd rows: the strength of the pressure wave is 195 kPa; 3rd to 6th rows: the strength of the pressure wave is 265 kPa; 7th and 8th rows: the strength of the pressure wave is 550 kPa (the counter jet is indicated by an arrow). The time interval between images is 1/2000 second.

D. Bubble Collapse Flows at $\gamma \approx 1$

The other critical value for the formation of the counter jet occurs at $\gamma \approx 1$ where the bubble surface is close to the solid boundary. For this relatively low stand-off, a thin fluid layer exists in the small gap

between the bubble surface and the rigid boundary. In order to understand the characteristics of the flow fields under this critical condition, experiments at both locations where γ is slightly greater than and equal to one are performed.

The bubble collapse flow induced by a pressure wave of 320 kPa at the stand-off distance γ slightly greater than 1 is performed first. The bubble deformed and changed from a bowl-like shape to the toroidal shape after the liquid jet threads the bubble surface, as shown in the first row of Figure 8. The diameter of the liquid jet is larger than the larger stand-off experiments presented before. Although the gap between the bubble surface and the solid boundary is small, a stagnation ring is still formed after the liquid jet impacts the solid boundary. The outwards radial flow collides with the flow induced by the still contracting bubble and a splash is projected away from the boundary, as shown in the schematic diagram of Figure 8. The liquid layer in the gap inside the stagnation ring is squeezed inwards to form the counter jet, as shown in the third row and the schematic diagram of Figure 8. Finally the bubble is broken into small bubbles.
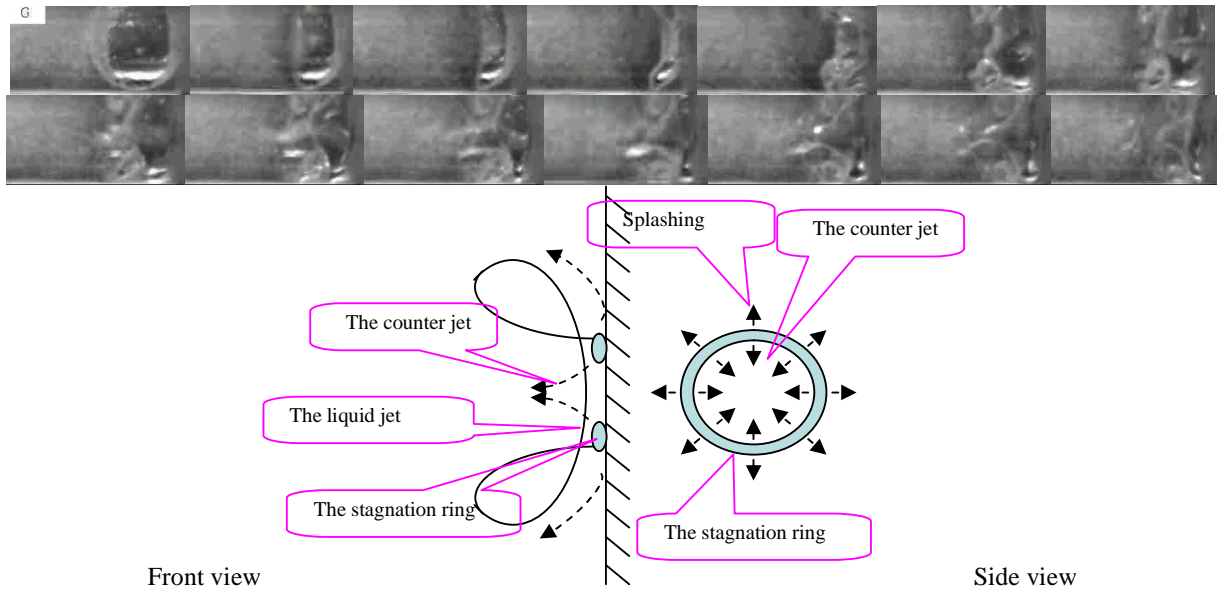
Fig. 8. Upper Part: Images of the bubble collapse at γ ≈ 1 (the counter jet is indicated by an arrow). The strength of the pressure wave is 320kPa. The time interval between images is 1/2000 second; Lower Part: Schematic diagram for the formation of the counter jet and the splashing.

For the stand-off distance γ = 1, the deformed bubble does not become toroidal since the liquid jet can not thread the bubble surface but just push the front and the rear bubble surfaces to be overlaid on the solid boundary. After the liquid jet impacts the solid boundary, it just splashes along the radial direction. The bubble collapses subsequently along the radial direction without forming the stagnation ring and the counter jet, as the images and the schematic diagram shown in Figure 9.

For all the experiments performed in this study, the strength of the pressure wave adopted to induce the bubble collapse flow is kept as low as possible so that the bubble collapsed in a longer period of time. The characteristics of the bubble collapse flows at different stand-off distances can thus be clearly manifested. However, different strengths of the pressure waves are needed to induce the bubble collapse flow at different γ locations. A lower strength of the pressure wave is needed for an increasing γ value and vise versa.
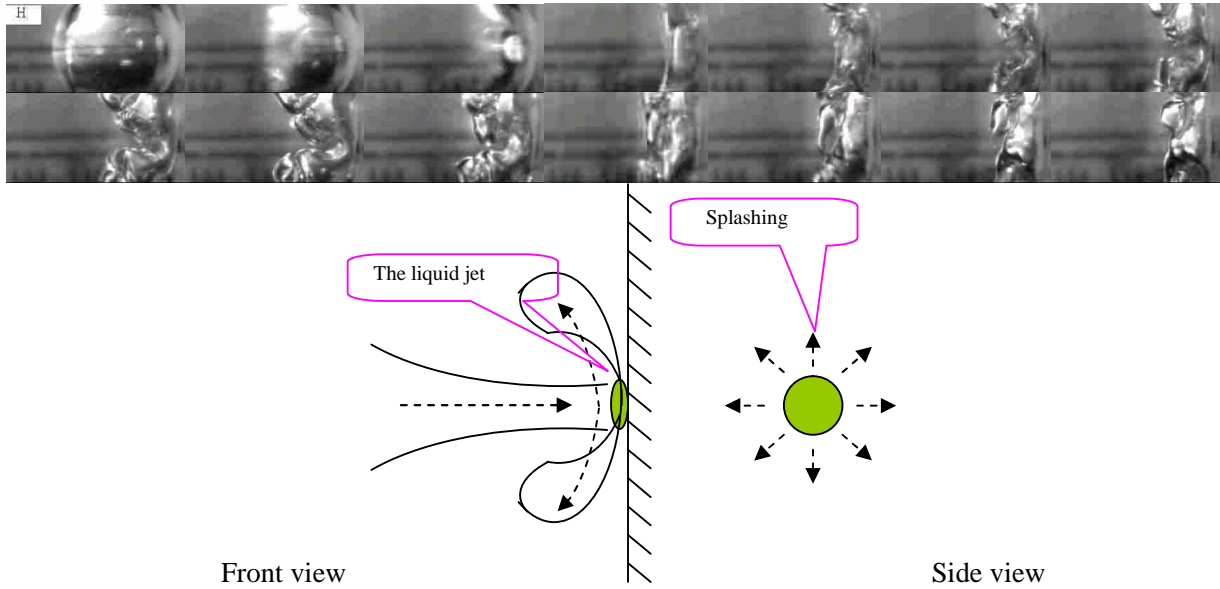
Fig. 9**. Upper Part: Images of bubble collapse at γ = 1; the strength of the pressure wave is 520 kPa; the time interval between images is 1/2000 second; Lower Part: Schematic diagram of the liquid jet and the splashing.**

CONCLUSION

In this study, a single cavitation bubble is generated by rotating a U-tube filled with water; the pressure at the rotating axis of the U-tube is lowered to the water vapor pressure due to the centrifugal acceleration, and the cavitation bubble is generated right at the rotating axis. The bubble collapse flows are induced by the pressure waves of different strengths. Sequential images of the bubble collapse flow are recorded by a high speed camera. The characteristics of the cavitation bubble collapse flow are clearly manifested by the cinematographic analyses.

For a large stand-off distance, $\gamma \approx 7$, the bubble collapsed without solid boundary influence, a liquid jet is formed due to the bubble deformation. The liquid jet then penetrates the bubble surface. The Kelvin-Helmholtz instability occurs around the penetrated jet surface and vortices are formed due to the presence of sufficient velocity shear between the jet flow and the surrounding static fluid. Counter jet is not formed for such a stand-off distance.

For the stand-off distance, $\gamma \approx 2$, which falls within the range $1 < \gamma \le 3$, the penetrated jet is capable to impact the solid boundary. A stagnation ring is formed on the solid boundary which separates the jet into an outwards and inwards radial flow. The liquid between the bubble surface and the solid boundary is squeezed by the inwards radial flow to form the counter jet.

At the critical stand-off distance, $\gamma \approx 3$, whether the counter jet occurs depends on the strength of the pressure wave used to induce the bubble collapse. For a lower strength pressure wave, the liquid jet penetrates the bubble but is not able to impact the solid boundary. Neither stagnation nor counter jet can be generated. For an intermediate strength pressure wave, the penetrated jet spread radially so that the circumference of the jet touch the tube wall before the jet front impacts the solid boundary. Neither stagnation ring nor counter jet can be generated. If the strength of the pressure wave is further increased,

the penetrated jet is able to impact the solid boundary directly to form the stagnation ring and the counter jet.

For the stand-off distance γ slightly greater than 1, a thin liquid layer exists in the small gap between the bubble surface and the solid boundary. The penetrated jet impacts the boundary directly. The stagnation ring is formed on the solid boundary. The thin liquid layer inside the stagnation ring is squeezed by the inwards radial flow to form the counter jet. If γ is equal to 1, the bubble surface is in contact with the solid boundary, the liquid jet can not penetrate the bubble but splashes along the radial direction without forming the stagnation ring and the counter jet.

The complex phenomenon of cavitation bubble collapse flows are clearly manifested by the cinematographic analyses performed in this study.

REFERENCES

Akhatov I, Lindau O, Topolnikov A, Mettin R, Vakhitova N, Lauterborn W (2001), "Collapse and rebound of a laser-induced cavitation bubble," Physical of Fluids 13: 2805-2819.

Akmanov AG, Ben'kovskii VG, Golubnichii PI, Maslennikov SI, Shemanin VG (1974), "Laser sonoluminescence in a liquid," Soviet Physics Acoustics 19: 417–418.

Baghdassarian O, Chu HC, Tabbert B, Williams GA (2001), "Spectrum of luminescence from laser-created bubbles in water," Physical Review Letters 86: 4934–4937.

Benjamin TB, Ellis AT (1966), "The collapse of cavitation bubbles and the pressures thereby produced against solid boundaries," Philosophical Transactions of the Royal Society of London Series A, Mathematical and Physical Sciences 260: 221–240.

Best JP (1993), "The formation of toroidal bubbles upon the collapse of transient cavities," Journal of Fluid Mechanics 251: 79–107.

Blake JR, Hooton MC, Robinson PB, Tong RP (1997), "Collapsing cavities, toroidal bubbles and jet impact. Philosophical Transactions Mathematical," Physical and Engineering Sciences 355: 537–550.

Brujan EA, Keen GS, Vogel A, Blake JR (2002), "The final stage of the collapse of a cavitation bubble close to a rigid boundary," Physics of Fluids 14: 85–92.

Buzukov AA, Teslenko VS (1971), "Sonoluminescence following focusing of laser radiation into liquid," Journal of Experimental and Theoretical Physics Letters 14: 189–191.

Gilmore FR (1952), The growth and collapse of a spherical bubble in a viscous compressible liquid. Technical Report California Institute of Technology, Pasadena, CA.

Harrison M (1952), "An experimental study of single bubble cavitation noise," The Journal of the Acoustical Society of America 24: 776-782.

Kling CL, Hammitt FG (1972), "A photographic study of spark-induced cavitation bubble collapse," Transactions of the ASME D: Journal of Basic Engineering 94: 825–833.

Kodama T, Tomita Y (2000), "Cavitation bubble behavior and bubble-shock wave interaction near a gelatin surface as a study of in vivo bubble dynamics," Applied Physical B 70: 139–149.

Kornfeld M, Suvorov L (1944), "On the destructive action of cavitation," Journal of Applied Physics 15: 495-506.

Lauterborn W (1972), "High-speed photography of laser-induced breakdown in liquids," Applied Physical Letters 21: 27–29.

Lauterborn W (1974), "Kavitation durch laserlicht," Acustica 31: 52–78.

Lindau O, Lauterborn W (2003), "Cinematographic observation of the collapse and rebound of a laser-produced cavitation bubble near a wall," Journal of Fluid Mechanics 479: 327–348.

McCarn AR, Englert EM, Williams GA (2006), Laser-Induced Bubbles in Glycerol-Water Mixtures. UCLA Physics and Astronomy Research.

Naude CF, Elli AT (1961), "On the mechanism of cavitation damage by nonhemispherical cavities collapse in contact with a solid boundary," Transactions of the ASME D: Journal of Basic Engineering 83: 648-656.

Ohl CD, Philipp A, Lauterborn W (1995), "Cavitation bubble collapse studied at 20 million frames per second," Annalen der Physik 4: 26-34.

Ohl CD, Lindau O, Lauterborn W (1998), "Luminescence from spherically and aspherically collapsing laser induced bubbles," Physical Review Letters 80: 393-397.

Ohl CD, Kurz T, Geisler R, Lindau O. Lauterborn W (1999), "Bubble dynamics, shock waves and sonoluminescence," Philosophical Transactions: Mathematical, Physical and Engineering Sciences 357: 269–294.

Philipp A, Delius M, Scheffczyk C, Vogel A, Lauterborn, W (1993), "Interaction of lithotripter-generated shock waves with air bubbles," The Journal of the Acoustical Society of America 93: 2496-2509.

Philipp A, Lauterborn W (1998), "Cavitation erosion by single laser-produced bubbles," Journal of Fluid Mechanics 361: 75–116.

Plesset MS (1949), "The dynamics of cavitation bubbles," Trans. ASME: Journal of Applied Mechanics 16: 277–282.

Plesset MS, Zwick SA (1952), "A nonsteady heat diffusion problem with spherical symmetry," Journal of Applied Physics 23: 95–98

Plesset MS, Chapman RB(1971), "Collapse of an initially spherical vapour cavity in the neighbourhood of a solid   boundary," Journal of Fluid Mechanics 47: 283–290.

Raleigh L (1917), "On the pressure developed in a liquid during the collapse of a spherical cavity," Philosophical Magazine, 34: 94–98.

Shaw SJ, Jin YH, Schiffers WP, Emmony DC (1996), "The interaction of a single laser-generated cavity in water with a solid surface," The Journal of the Acoustical Society of America 99: 2811–2824.

Shaw SJ, Schiffers WP, Emmony DC (2001), "Experimental observations of the stress experienced by a solid surface when a laser-created bubble oscillates in its vicinity," The Journal of the Acoustical Society of America 110: 1822–1827.

Sankin GN, Simmons WN, Zhu SL, Zhong P(2005), "Shock wave interaction with laser- generated single bubble," Physical Review Latter 034501: 1~4.

Tomita Y, Shima A (1986), "Mechanisms of impulsive pressure generation and damage pit formation by bubble collapse," Journal of Fluid Mechanics 169: 535-564.

Tong RP, Schiffers WP, Blake SJ (1999), "Splashing in the collapse of a laser-generated cavity near a rigid boundary," Journal of Fluid Mechanics 380: 339-361.

Vogel A, Lauterborn W (1988), "Time-resolved particle image velocimetry used in the investigation of cavitation bubble dynamics," Applied Optics 29: 1869-1876.

Vogel A, Lauterborn W, Timm R (1989), "Optical and acoustic investigations of the dynamics of laser-produced cavitation bubbles near a solid boundary," Journal of Fluid Mechanics 206: 299–338.

Ward B, Emmony DC (1991), "Direct observation of the pressure developed in a liquid during cavitation-bubble collapse," Applied Physics Letters 59: 2228–2231.

Wolfrum B, Kurz T, Lindau O, Lauterborn W (2001), "Luminescence of transient bubbles at elevated ambient pressure," Physical Review E 64: 046306-5.

Zhang S, Duncan JH, Chahine GL (1993), "The final stage of the collapse of a cavitation bubble near a rigid wall," Journal of Fluid Mechanics 257: 147–181.

Zhu S, Zhong P (1999), "Shock wave–inertial microbubble interaction: A theoretical study based on the Gilmore formulation for bubble dynamics," The Journal of the Acoustical Society of America 106: 3024-2033.